ACS OMEGA

Open Access

http://pubs.acs.org/journal/acsodf

Article

Influence of Biotite Content on the Mechanical Response of Granite Using a Novel Three-Dimensional Grain-Based Model and Force Chain Analysis

Peigang Geng, Fangbin Zhao, Wei Li,* Jie Zhang, and Jingwei Liu

Cite This: *ACS Omega* 2024, 9, 9603−9614

Read Online

ACCESS | Metrics & More | Article Recommendations

ABSTRACT: In this study, a three-dimensional grain-based model based on the discrete element method is utilized to replicate the heterogeneous structure of crystalline granite, and corresponding laboratory tests are conducted to validate the numerical conclusions. A novel model and an analytical method involving a multilevel force chain network are employed to quantitatively investigate the influence of mineral content on the mechanical behavior of granites. First, a set of granite specimens with varying biotite contents is constructed, and then, uniaxial compression tests are conducted. The effects of the mineral content on the mechanical behavior, force chain network characteristics, and fracture resistance of granite specimens are quantitatively analyzed. The results indicate an inverse relationship between the biotite (V_B) content and the load-bearing capacity of granite under uniaxial compression conditions. As V_B increases, the number of contacts within the biotite structure increases, as does the force chain distribution density within the biotite structure, while the force chain distribution density in other intragranular structures correspondingly decreases. The average values and sum values of all of the force chains in the whole specimen decrease with increasing V_B. Among the various structures, intragranular structures exhibit the highest fracture resistance, whereas intergranular structures exhibit lower resistance.

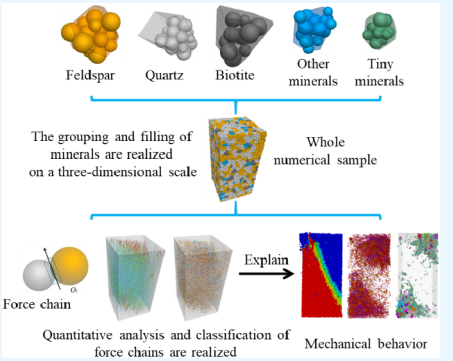

1. INTRODUCTION

Granite, as a primary constituent of igneous rocks, is a fundamental rock type that forms the Earth's continental crust and plays a crucial supporting role in engineering applications.[1,2] Characterized as a typical crystalline rock, granite's internal structure is generally composed of various types of crystalline minerals.[3−5] In general, there are substantial differences in the load-bearing capacity and fracture resistance among various types of minerals.[6] Therefore, the internal heterogeneity of these materials is closely related to their mechanical behavior.[7] Examining the impact of the mineral content in the crystalline structure of granite on its mechanical behavior and fracture characteristics holds great significance.

Many laboratory tests have been conducted to investigate the influence of mineral content on the mechanical behavior of rock materials and have yielded valuable conclusion.[8,9] However, due to the limitations of testing technology in laboratory tests, experimental studies on granite are often confined to describing the variations in macroscopic mechanical parameters, such as compressive strength,[10] tensile strength,[11] elastic modulus,[12] crack behavior,[13] and failure mode.[14] The microscopic mechanisms of damage and failure in granite under loading, such as the characteristics of microcracks and force chain distribution, cannot be quantitatively analyzed. Leveraging the rapid development of computer technology, numerical simulation has gradually become a powerful tool for researchers studying the mechanical properties of rock material.[15−18] The particle flow code (PFC), developed by Itasca and based on the discrete element method, has been widely applied in rock mechanics and has achieved many useful results.[19,20] Due to the advantages of low modeling difficulty and fast calculation speed, two-dimensional homogeneous models and three-dimensional homogeneous models have been widely used in the investigation of microfracture information, such as the velocity field, strain field, and microcrack field, of samples under loading.[21,22] In these homogeneous models, all the elements and contacts are calibrated by the same microscopic parameters, rendering the entire numerical specimen completely homogeneous.[23,24] This limitation prevents reproduction of the heterogeneous structure of granite, thus imposing significant constraints on the interpretation of its mechanical behavior.

Received: November 29, 2023
Revised: February 5, 2024
Accepted: February 6, 2024
Published: February 16, 2024

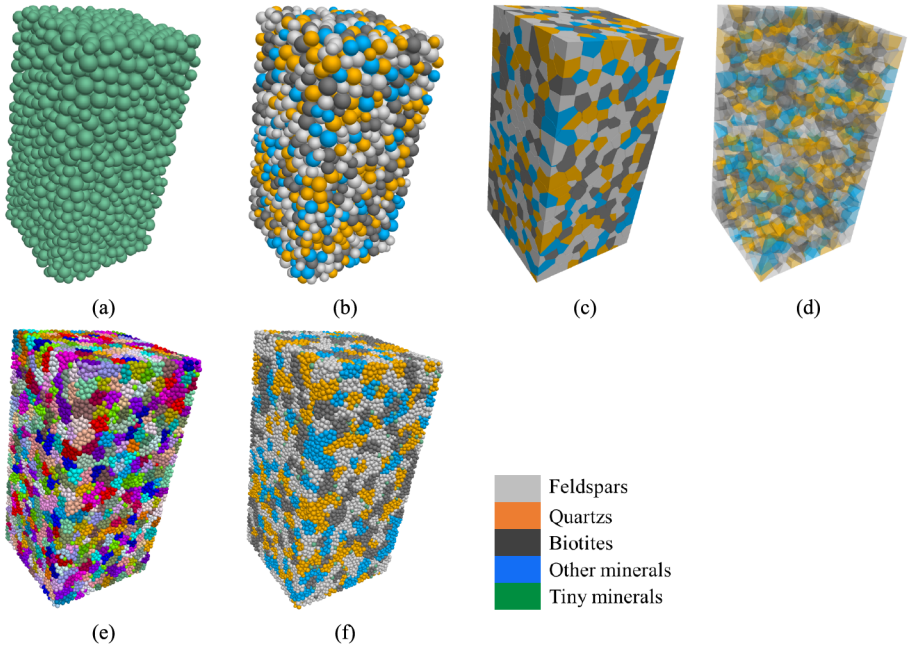

Figure 1. Flowchart of the generation of PFC3D-GBM: (a) initial particle-based models; (b) grouping of basic elements; (c) assembly of block units; (d) assembly of geometry units; (e) division of the geometric range of mineral grains; (f) grouping of mineral grains.

To better reproduce the heterogeneous structure of rocks, Potyondy et al.[25] established the grain-based model (GBM) based on the PFC in 2004. This model not only reproduces the interactions between mineral grains but also simulates the mechanical behavior within a single grain. In recent years, many scholars have improved GBMs based on the PFC and applied them to obtain information about microscopic mechanisms that are not available in laboratory tests.[26−30] Currently, most GBMs are constructed in two dimensions, with only a few models capable of grouping and filling mineral grains in three dimensions,[31−33] providing a more realistic representation of the internal crystalline structure of granite. Furthermore, in these studies, the analysis methods used are relatively limited, and a suitable and powerful tool for linking the macroscopic mechanical behavior of specimens with microscopic mechanism information has not been found.

In discrete materials, internal particles are arranged nonuniformly. A local concentrated stress can form between these particles under loading, resulting in a complete and complex force chain network for the whole numerical sample. A force chain network provides the most critical information for particle-based materials.[34−36] It is the crucial factor inducing the load-bearing capacity, deformation characteristics, microfracture behavior, and macrofracture mode of samples.[37,38] The reliability of using force chain networks to explain changes in the mechanical behavior of rock materials during loading has been acknowledged by many scholars.[23,39−41] However, due to limitations in modeling and subsequent analysis methods, quantitative analysis of force chain networks has rarely been performed. Additionally, the differences in mechanical behavior between various intragranular and intergranular structures within granites inevitably lead to different levels of corresponding force chain networks. This heterogeneity in force chain networks needs to be considered. Most existing analyses treat the force chain network as a whole,[42−44] which is inappropriate when explaining the mechanical behavior of crystalline rocks such as granite.

In this study, a three-dimensional grain-based model based on the discrete element method was utilized to replicate the heterogeneous structure of the crystalline granite. In this model, not only is the mechanical behavior of different types of minerals distinguished, but also the force chain network realizes multilevel classification and quantitative analysis. Both the novel model and force chain analysis method were employed to quantitatively investigate the influence of the mineral content on the mechanical behavior of granites. First, a set of granite specimens with varying biotite contents was constructed, and then, a uniaxial compression test was conducted. The effects of the mineral content on the mechanical behavior, force chain network characteristics, and fracture resistance of granite specimens were quantitatively analyzed.

2. INVESTIGATION METHODOLOGY

2.1. Model Construction Process. Figure 1 illustrates the specific construction process of the model:[7,45]

(a) Step A: as shown in Figure 1a, an initial particle-based model is constructed in which the particle sizes are relatively large, representing the mineral grains.

(b) Step B: as shown in Figure 1b, the granite used in this study is sourced from Huanggang city, Hubei Province, China. According to the XRD results, the mineral composition and corresponding volume fractions are as follows: feldspar (43.20%), quartz (35.52%), biotite (11.52%), other minerals (5.76%), and minute minerals (4.00%). Based on these results, the particles are grouped to represent different types of minerals, each labeled with a corresponding color.

(c) Step C: as shown in Figure 1c, the grouped particles are transformed to block elements.

(d) Step D: as shown in Figure 1d, block elements are converted to geometric elements to facilitate the subsequent filling of mineral grains.

https://doi.org/10.1021/acsomega.3c09304
ACS Omega 2024, 9, 9603−9614

(e) Step E: as shown in Figure 1e, the geometric elements are filled with basic unit elements.

(f) Step F: as shown in Figure 1f, at this point, the mineral grains are successfully grouped and filled in three dimensions, effectively reproducing the heterogeneous structure of granite.

In this study, the specimens used in the laboratory test and numerical simulations are rectangular prisms with dimensions of 50 × 50 × 100 mm subjected to uniaxial loading.

2.2. Contact Classification. The key distinction between heterogeneous and homogeneous models lies in the ability of heterogeneous models to classify contacts based on predefined mineral types with corresponding micromechanical parameters assigned. As shown in Figure 2a, all contacts in this model are

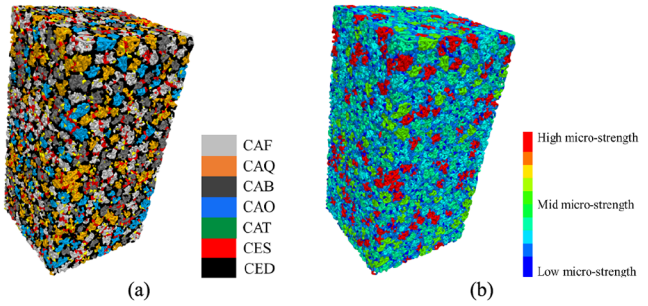

Figure 2. Classification of contacts: (a) grouping of contacts; (b) microstrength distribution.

classified into intragranular contacts, including contacts in feldspar (CAF), quartz (CAQ), biotite (CAB), other minerals (CAO), minute minerals (CAT), and intergranular contacts, including contacts between the same minerals (CES) and between different minerals (CED). As shown in Figure 2b, the microstrength of various types of contacts in the numerical sample is different.

2.3. Force Chain Classification. In addition to contacts, the internal force chain network during loading in this model is also classified. All force chains are categorized into internal force chains of feldspar, quartz, biotite, other minerals, and minute minerals; force chains between the same mineral types; and force chains between different mineral types.

2.4. Model Validity Verification. In this GBM, intragranular and intergranular contacts utilize the parallel bond model (PBM) to reproduce microscopic-scale fracture behavior in rock materials.[45,46] The final calibrated microscopic parameters are listed in Table 1.

The microscopic parameters within the model are calibrated using the 'trial and error' method, which is widely applied and effective.[6,7,23,47] The main calibration steps are as follows: (1) fundamental mechanical tests are conducted to determine the macroscopic mechanical parameters of real rock materials, such as compressive strength, tensile strength, and elastic modulus; (2) the approximate ranges of the microparameters of various minerals in the numerical sample are determined by reference and experience; (3) the corresponding simulation tests are conducted, and the internal microscopic parameter values of the numerical samples are gradually adjusted according to the laboratory test results; and (4) a set of microscopic parameters that can reproduce the real mechanical properties of the rock materials is obtained.

As shown in Figure 3a, real samples and simulated samples were prepared, and the real samples are subjected to uniaxial compression using a mechanical testing system 816. The

Table 1. Microparameters of Grain-Based Model

microparameters	feldspars	quartz	biotites	others	tiny/fine minerals
Mineral grains					
volume composite (%)	43.20	35.52	11.52	5.76	4.0
minimum grain radius R_G (mm)	1.80				0.65
ratio of maximum to minimum grain radius r_G	1.60				1.60
Basic elements					
minimum particle radius R_P (mm)	0.65				
ratio of maximum to minimum particle radius r_P	1.60				
Young modulus (GPa)	55.0	70.0	40.0	35.0	30.0
stiffness ratio	1.6	1.4	1.8	2.0	2.2
Intragranular contacts					
Young modulus (GPa)	55.0	70.0	40.0	35.0	30.0
cohesion strength (MPa)	320.0	360.0	160.0	120.0	80.0
tension strength (MPa)	160.0	180.0	80.0	60.0	40.0
stiffness ratio	1.6	1.4	1.8	2.0	2.2
friction angle (°)	14	12	16	18	22

Intergranular Contacts	between same minerals	between different minerals
Young modulus (GPa)	2.5	2.2
cohesion strength (MPa)	50.0	40.0
tension strength (MPa)	25.0	20.0
stiffness ratio	2.6	2.8
friction angle (°)	26	28

loading rate was 0.0015 mm/s. In the numerical simulation, the loading plate is used to simulate uniaxial compression. Figure 3b compares the load−displacement curves of the laboratory test and numerical simulation under uniaxial compression conditions. Both curves exhibit consistent trends, capturing elastic deformation, nonlinear deformation, and postpeak drop stages. In terms of the macroscopic mechanical parameters, as listed in Table 2, the experimental and simulated values for the peak load are 247.20 kN and 251.96 kN, respectively, and the experimental and simulated values for the elastic modulus are 9.18 and 8.85 GPa, respectively, indicating minimal error. The numerical curve does not exhibit a densification stage in the initial phase, which results in a slightly lower displacement at the peak load moment. This phenomenon is acceptable in PFC simulations[21] and does not affect the validity of the model. The experimental results and simulation results of the failure mode are in good agreement, and the overall failure mode is obvious failure of the upper and lower end faces.

3. NUMERICAL SPECIMENS WITH DIFFERENT BIOTITE CONTENTS

3.1. Numerical Specimens. To investigate the influence of mineral content on the deformation characteristics and mechanical behavior of granite, in this study, a series of specimens with varying biotite contents, V_B, are constructed. The specific values for different mineral contents are listed in Table 3. The V_B content ranges from 9.6% to 67.2%, while the

https://doi.org/10.1021/acsomega.3c09304
ACS Omega 2024, 9, 9603−9614

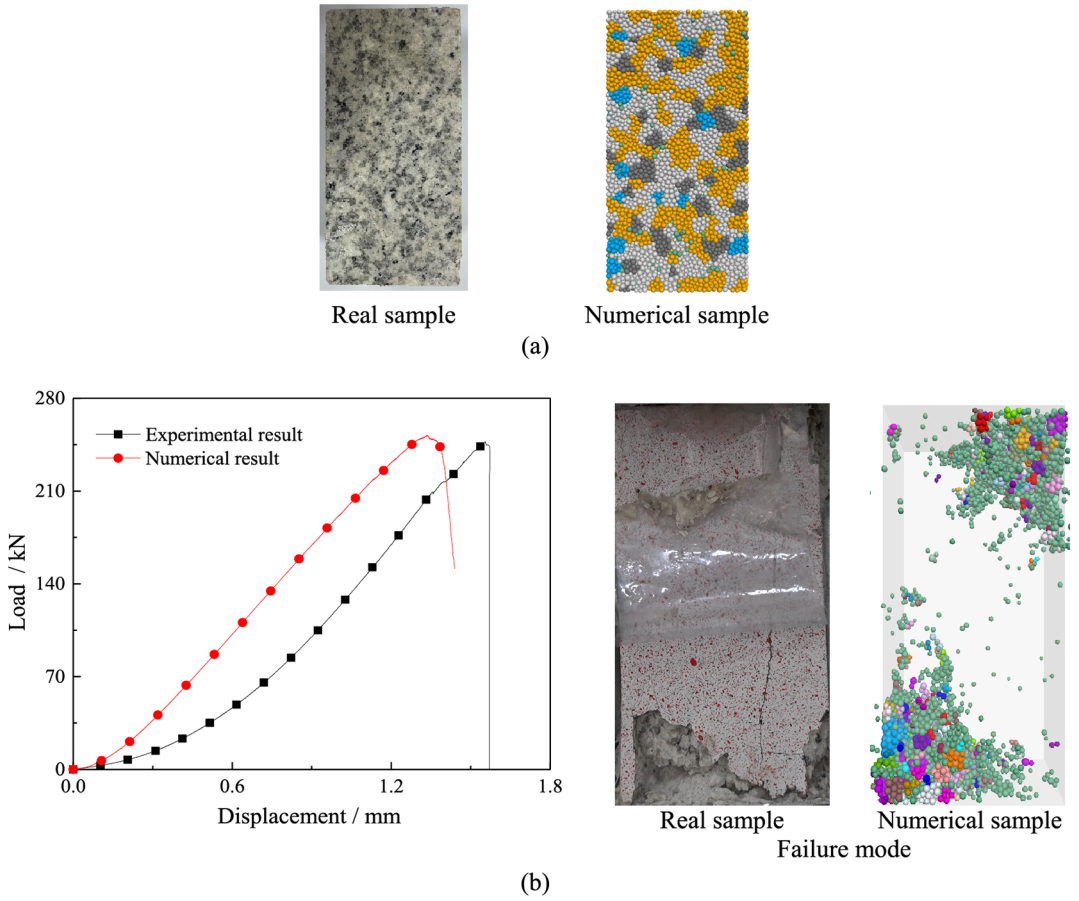

Figure 3. Verification of microparameters and model validity: (a) intact real sample and numerical sample; (b) comparison between experimental results and numerical results.

Table 2. Macroscopic Mechanical Parameters of Real Sample and Numerical Sample

parameters	experimental results	numerical results	error (%)
peak load (kN)	247.20	251.96	1.91
elastic modulus (GPa)	9.18	8.85	3.66
displacement at the peak load moment (mm)	1.56	1.33	15.92

Table 3. Volume Proportions of Various Minerals in the Numerical Samples

group	feldspars (%)	quartz (%)	biotites (%)	others (%)	tiny minerals (%)	total minerals (%)
no. 1	43.2	28.8	9.6	14.4	4.0	100.0
no. 2	36.0	24.0	24.0	12.0	4.0	100.0
no. 3	28.8	19.2	38.4	9.6	4.0	100.0
no. 4	21.6	14.4	52.8	7.2	4.0	100.0
no. 5	14.4	9.6	67.2	4.8	4.0	100.0

proportions of feldspar, quartz, and other minerals remain constant at 3:2:1, and the minute minerals maintain a constant content of 4.0%.

Figure 4 illustrates the grouping and contact distribution of the mineral grains for different V_B specimens. As V_B increases, the volume of dark gray biotite markers significantly increases, accompanied by a noticeable increase in the number of internal contacts within biotite minerals.

3.2. Numbers of Basic Elements and Contacts. Figure 5 quantitatively depicts the variation in the number of basic elements (N_B) representing different mineral types with changing V_B. As the V_B content increases from 9.6% to 67.2%, the numbers of basic elements in feldspar, quartz, and other minerals decrease from 29299, 18460, and 9297 to 9413, 6334, and 3138, with decreases of 67.87%, 65.69%, and 66.25%, respectively. In contrast, the number of basic elements in biotite increases from 6177 to 44325, with an increase of 617.58%. The number of basic elements in minute minerals is approximately 2400.

Figure 6 shows the changes in the number of various contacts (N_C) with varying V_B. In Figure 6a, as V_B increases from 9.6% to 67.2%, the number of contacts within feldspar, quartz, and other minerals decreases from 59671, 40980, and 20730 to 20984, 14082, and 7069, corresponding to decreases of 64.83%, 65.64%, and 65.90%, respectively. Moreover, the number of contacts within biotite increases from 13685 to 98694, indicating an increase of 621.18%. The number of internal contacts for minute minerals does not fluctuate significantly with changing V_B and remains at approximately 400. Figure 6b shows that as V_B increases from 9.6% to 67.2%, the number of contacts between the same minerals increases from 37968 to 54362, with a 43.18% increase, while the number of contacts between different minerals decreases from 91845 to 69647, with a 24.17% decrease.

https://doi.org/10.1021/acsomega.3c09304
ACS Omega 2024, 9, 9603−9614

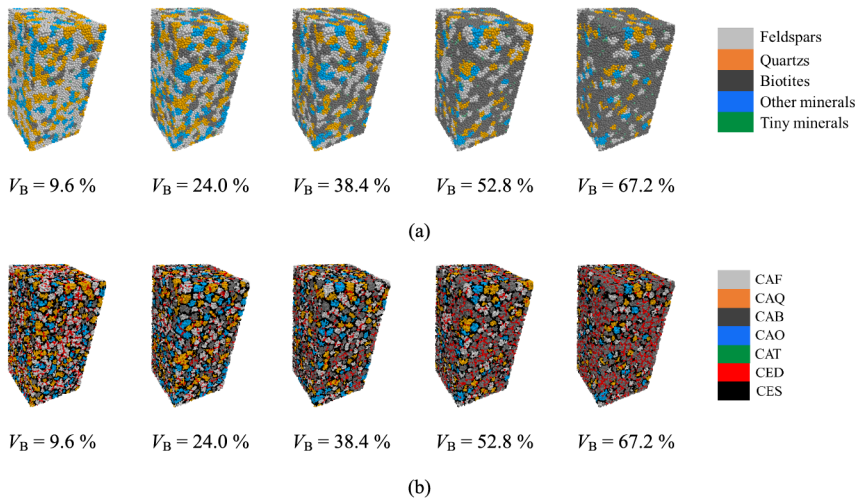

Figure 4. Mineral distribution and contact distribution of samples with different biotite contents: (a) mineral distribution; (b) contact distribution.

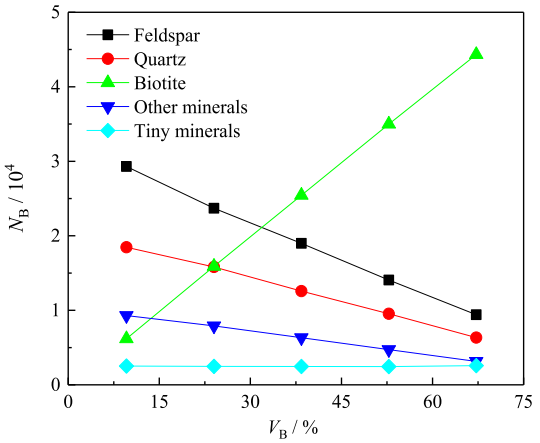

Figure 5. Variation of the number of basic elements mimicking various minerals vs biotite content.

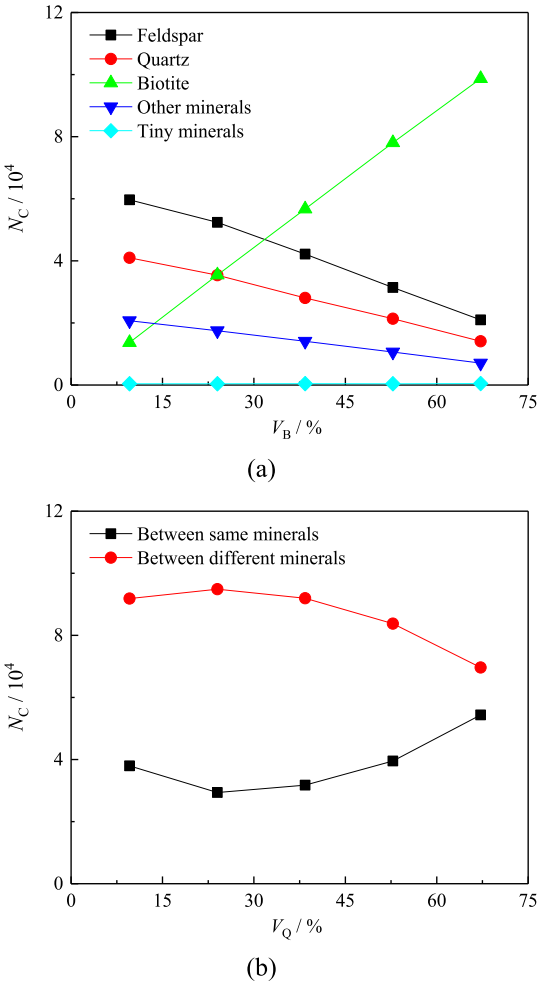

Figure 6. Variation of numbers of contacts in various structures versus biotite content: (a) various intragranular structures; (b) various intergranular structures.

4. MECHANICAL PROPERTIES

4.1. Load−Displacement Curve. The stress−strain curves of the numerical specimens with different V_B values are presented in Figure 7a. These curves exhibit consistent trends characterized by elastic deformation, nonlinear deformation, and a postpeak decline. The mineral content has a discernible impact on the macroscopic mechanical parameters. As V_B increases, the peak load of the specimens (P_{MAX}) decreases from 236.42 kN to 194.67 kN, representing a decrease of 17.66%, as illustrated in Figure 7b. The volumetric fraction of biotite is inversely proportional to the load-bearing capacity of the specimens under uniaxial compression conditions.

4.2. Microscopic Fracture Behavior. The number of cracks (N_c) within various intragranular structures is depicted in Figure 8a. The numbers of cracks in feldspar, quartz, other minerals, and minute minerals decrease from 4049, 1895, 10640, and 224 to 568, 475, 2124, and 184, respectively, as V_B increases from 9.6% to 67.2%. This corresponds to reductions of 85.97%, 74.93%, 80.04%, and 17.86%, respectively. Conversely, the number of cracks within biotite increases from 4168 to 16955, representing an increase of 306.79%. In terms of intergranular structures, as shown in Figure 8b, the number of cracks within the structures between the same mineral remains relatively constant as V_B increases from 9.6% to 67.2%. However, the number of cracks within the structures between different minerals decreases from 23859 to 10733, indicating a reduction of 55.01%.

https://doi.org/10.1021/acsomega.3c09304
ACS Omega 2024, 9, 9603−9614

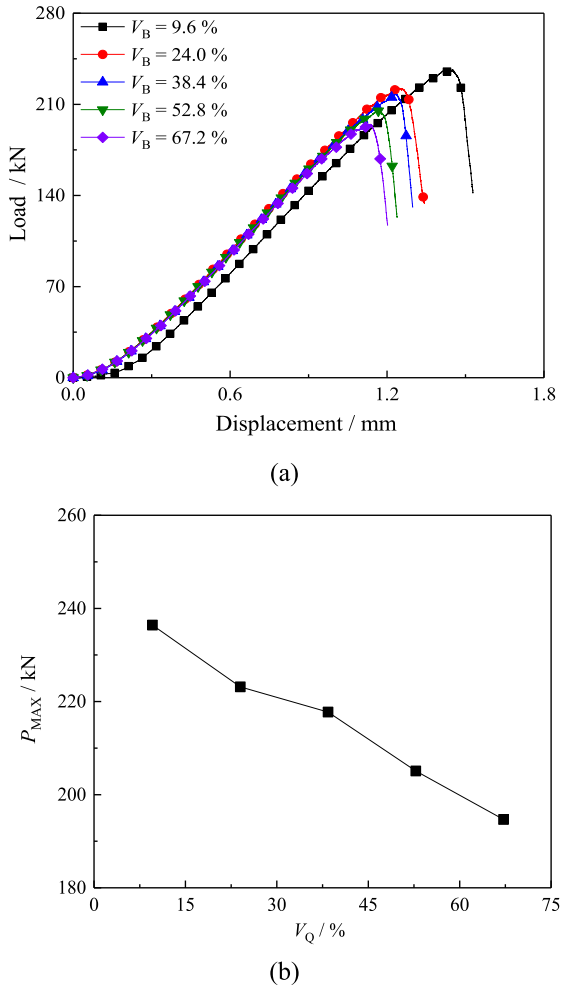

Figure 7. Macroscopic mechanical behavior of samples with different biotite contents: (a) load−displacement curve; (b) peak load.

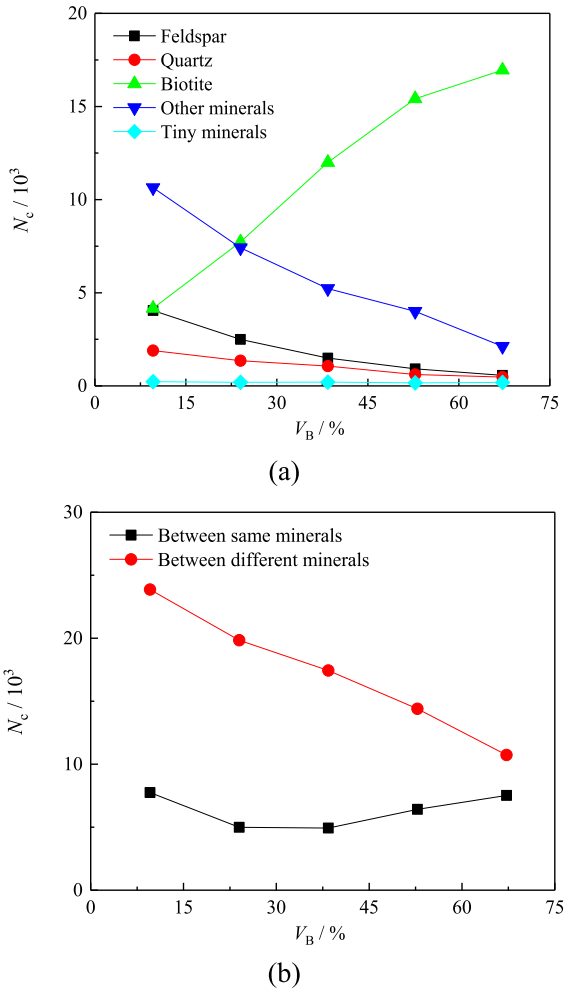

Figure 8. Variation of numbers of cracks in various structures versus biotite content: (a) various intragranular structures; (b) various intergranular structures.

5. FORCE CHAIN NETWORK CHARACTERISTICS

5.1. Overall Force Chain Network Level. The force chain networks, divided by the values at the moment of peak load under uniaxial compression conditions for different V_B values, are shown in Figure 9. According to the legend, the red force chain level is higher. As V_B increases, the number of red force chains within the specimens exhibits a slightly decreasing trend, indicating an overall decrease in the strength of the force chain network.

The trends in the average value (A_{FC}) and sum value (S_{FC}) of the force chains of all of the force chains with changing V_B are depicted in Figure 10. As V_B content continued to increase, the AFC decreased from 86.34 to 69.17 N, representing a decrease of 19.89%, while the S_{FC} decreased from 22.47 × 10^6 N to 18.07 × 10^6 N, indicating a reduction of 19.57%. Throughout this process, the peak load of the specimens consistently decreases. Thus, the overall strength of the specimens can be effectively characterized by the strength of the force chains.

5.2. Force Chains in Different Structures. Figure 11 shows the force chain distributions for the biotite structure and other intragranular structures, excluding biotite, categorized by force chain type. The density of the force chain distribution within the biotite structure significantly increases with an

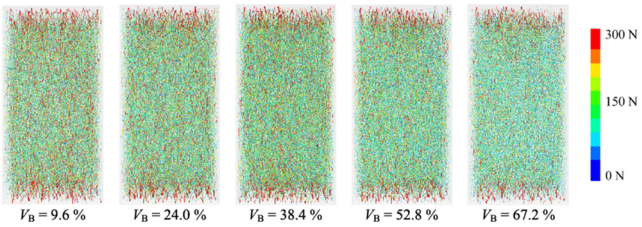

Figure 9. Force chain networks of samples with different biotite contents under uniaxial compression scaled by values at the peak load moment.

increasing V_B, while the density within other intragranular structures correspondingly decreases.

Regarding the quantity of force chains (N_{FC}), as shown in Figure 12a, when V_B increases from 9.6% to 67.2%, the number of force chains within the biotite structure increases from 13355 to 96956. Conversely, the force chain quantities in other intact minerals, namely, feldspar, quartz, and other minerals, all decrease from 59397, 40828, and 19684 to 20936, 14041, and 6816, respectively. Concerning intergranular structures, as depicted in Figure 12b, when V_B increases from 9.6% to 67.2%, the number of force chains within structures of the same mineral increases from 37256 to 53609. The number of force

https://doi.org/10.1021/acsomega.3c09304
ACS Omega 2024, 9, 9603−9614

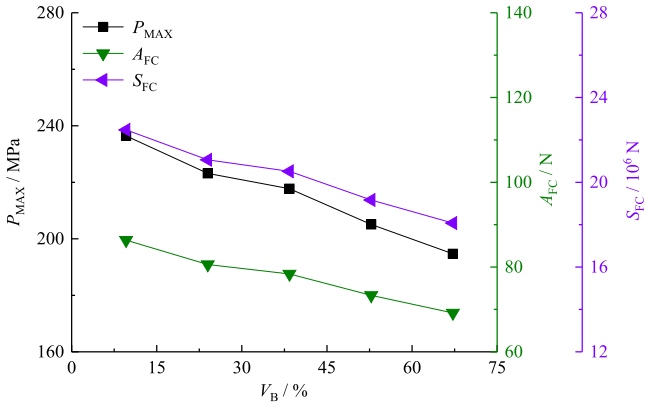

Figure 10. Variation of characteristic values of force chains of samples vs biotite content under uniaxial compression at the peak load moment.

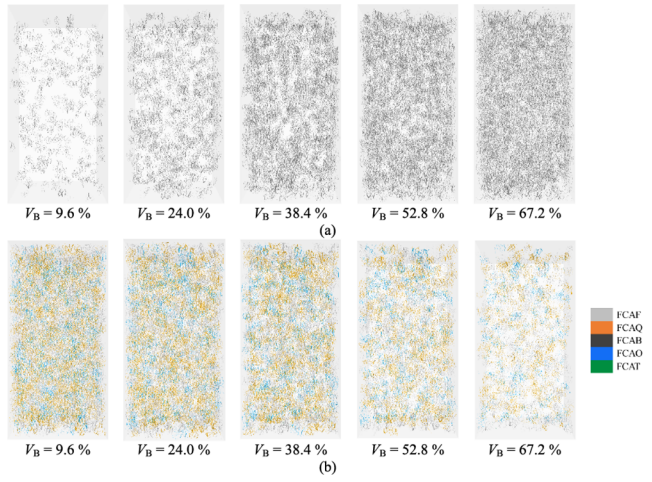

Figure 11. Force chain networks of samples with different biotite contents under uniaxial compression scaled by types at the peak load moment: (a) biotites; (b) various intragranular structures expect biotites.

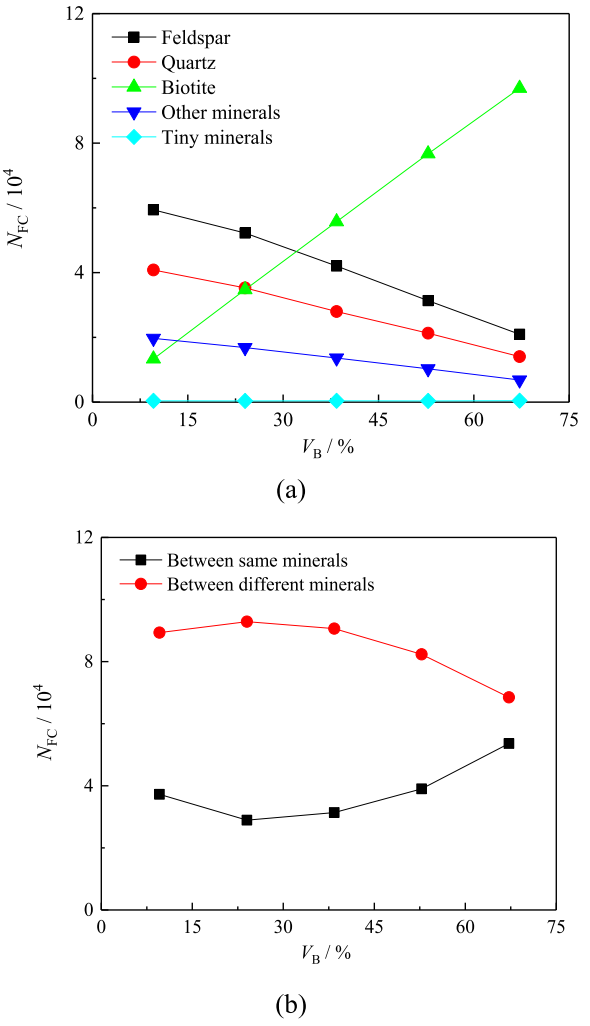

Figure 12. Variation of numbers of force chains in various structures versus biotite content at the peak load moment: (a) various intragranular structures; (b) various intergranular structures.

chains between structures of different minerals decreases from 89340 to 68493.

In terms of the sum values of the force chains (S_{FC}), as shown in Figure 13a, when V_B increases from 9.6% to 67.2%, the sum of the force chains within the biotite structure increases from 1.30 × 10^6 N to 8.20 × 10^6 N. Conversely, the sum of the force chains in the other intact minerals, including feldspar, quartz, and other minerals, all decrease from 6.70 × 10^6 N, 4.73 × 10^6 N, and 1.76 × 10^6 N to 1.85 × 10^6 N, 1.29 × 10^6 N, and 0.51 × 10^6 N, respectively. Concerning intergranular structures, as shown in Figure 13b, when V_B increases from 9.6% to 67.2%, the sum of the force chains within structures between the same mineral increases from 2.69 × 10^6 N to 2.94 × 10^6 N. Similarly, the sum of the force chains between structures of different minerals decreases from 5.34 × 10^6 N to 3.24 × 10^6 N.

In terms of the average values of the force chains (A_{FC}), as shown in Figure 14a, when V_B increases from 9.6% to 67.2%, the average value of the force chains within the biotite structure decreases from 97.55 to 84.59 N. Conversely, the average values of the force chains in other intact minerals, including feldspar, quartz, and other minerals, all decrease from 112.78, 115.76, and 89.57 N to 88.58, 92.24, and 75.13 N, respectively. Concerning intergranular structures, as shown in Figure 14b, when V_B increases from 9.6% to 67.2%, the average value of force chains within structures between the same mineral decreases from 70.54 to 54.90 N. The mean force chain value between structures of different minerals decreases from 59.77 to 47.37 N.

6. DISCUSSION: FRACTURE RESISTANCE

6.1. Fracture Resistance of Various Structures. At the microscopic scale, the initiation of cracks is a result of force chains acting on contacts. To provide a clearer description of the fracture resistance of structures from the perspective of force chains, we define the fracture resistance index (F). The specific calculation formula for the F value of structure A is as follows:

$$F_A = \frac{S_{FC\text{-}A}}{N_{c\text{-}A}} \quad (1)$$

in which F_A represents the fracture resistance index of structure A, and $S_{FC\text{-}A}$ and $N_{c\text{-}A}$ represent the sum of the force chains and the number of cracks in structure A, respectively. By this definition, a larger F value for a structure indicates that a greater number of force chains are required within a structure

https://doi.org/10.1021/acsomega.3c09304
ACS Omega 2024, 9, 9603−9614

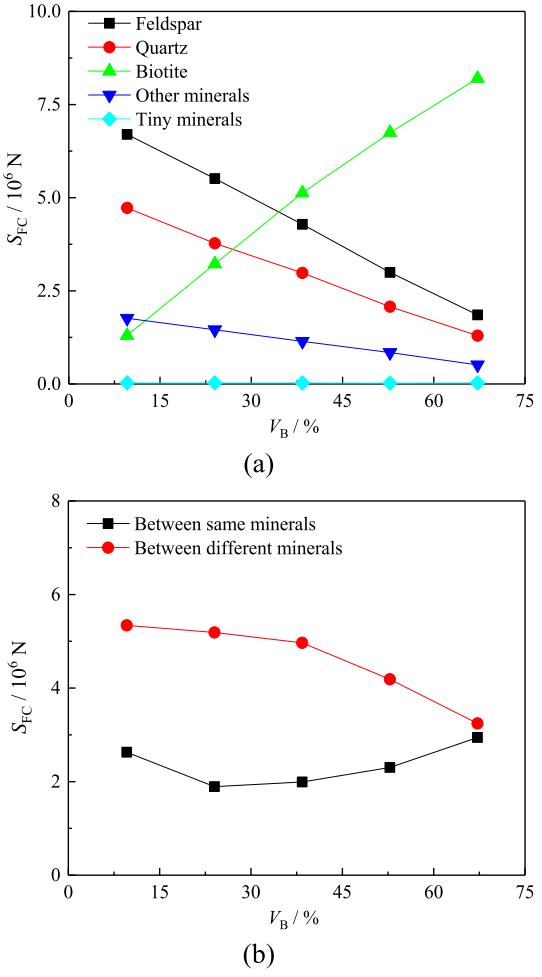

Figure 13. Variation of sum value of force chains in various structures versus biotite content at the peak load moment: (a) various intragranular structures; (b) various intergranular structures.

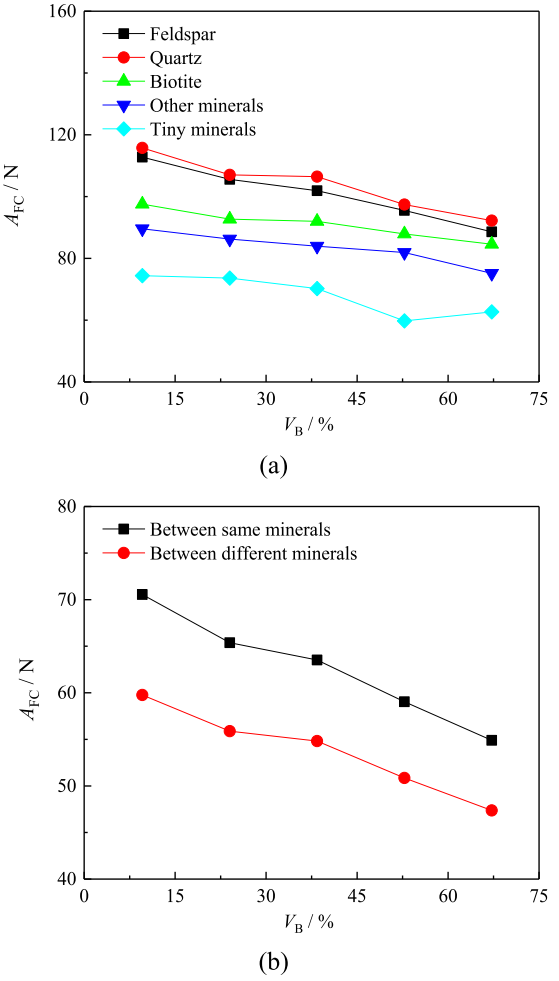

Figure 14. Variation of average value of force chains in various structures versus biotite content at the peak load moment: (a) various intragranular structures; (b) various intergranular structures.

to initiate a single crack. This implies a stronger fracture resistance for that structure.

Here, we calculate the fracture resistance index F for structures with different V_B values. As shown in Figure 15a, the fracture resistance of the intragranular structures is significantly greater than that of the overall structure and intergranular structures in these specimens. This implies that a higher level of force chains is required to initiate cracks within intragranular structures. Furthermore, within the various intragranular structures, as depicted in Figure 15b, feldspar and quartz exhibit significantly greater fracture resistance than do the other minerals. As illustrated in Figure 15c, the fracture resistance of structures made of the same minerals is significantly greater than that of structures made of different minerals.

As shown in Figure 16a, in the numerical sample in this study, the mineral structures are filled with numerous elements. Under the action of external loads, the contact between two adjacent basic elements breaks, and then microcracks occur. When the number of microcracks gradually increases, the sample experiences a complete crack field, after which macrocracks form. When the external load causes macroscopic fracturing of the sample, this load level is the peak load. Furthermore, the load threshold of fracture behavior in a certain type of mineral structure is proportional to the resistance to fracture, as shown in Figure 16b. The resistance to fracture of various mineral structures is ranked from largest to smallest according to quartz, feldspar, biotite, other minerals, and fine minerals. Therefore, the peak load of the sample is related to the volume proportion of these mineral structures with different fracture resistances. When the proportion of quartz is large, the sample is less prone to fracture and the peak load increases. In contrast, when the proportion of biotite inside the sample increases, macrofracturing occurs under a lower load, and then the peak load of the sample, that is, the load-bearing capacity decreases, which is also the situation in this study, as shown in Figure 16c.

6.2. Research Significance of the Force Chain Network. In PFC, the basic element is the most essential component of a discrete element sample. During loading, a certain value of concentrated stress, i.e., force chain O_F, is generated between two adjacent base elements to form bonds between the elements. This is a fundamental micromechanical behavior. Furthermore, in this model, the mineral structure is filled with basic elements, so the mechanical and fracture behaviors in the crystal can also be restored. Finally, the whole numerical sample is constructed of numerous basic elements, as shown in Figure 17a. Therefore, the force chain between adjacent basic elements is the most essential information in the numerical sample. As shown in Figure 17b, when a local

https://doi.org/10.1021/acsomega.3c09304
ACS Omega 2024, 9, 9603−9614

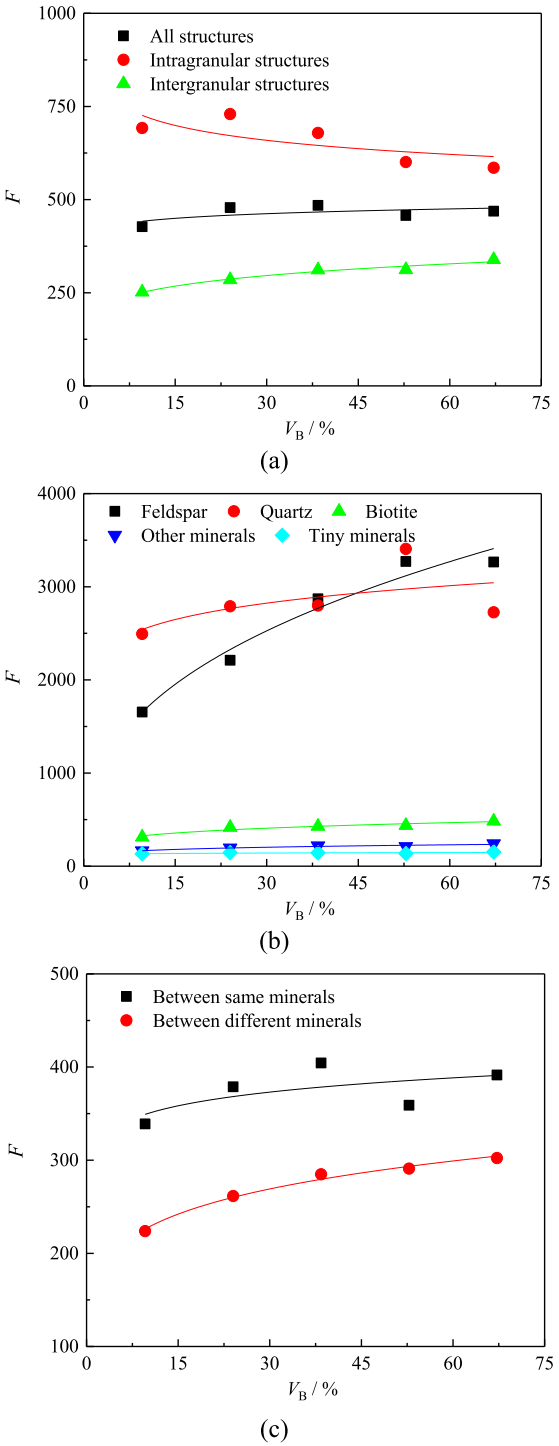

Figure 15. Variation of the resistance to fracture of various structures versus biotite content at the peak load moment: (a) all structures, intragranular structures, and intergranular structures; (b) various intragranular structures; (c) various intergranular structures.

particle cluster is loaded, a local force chain network is generated within it, and furthermore, the whole sample generates a complete force chain network. Under the action of this force chain network, the sample produces the corresponding mechanical response. The level of the force chain network in the upper and lower regions of the simulated sample is greater. Correspondingly, the displacement of the sample in these two regions is greater than that in the other regions, and more severe microfracture and macrofracture behaviors occur, which can be observed in the displacement field, crack field, and fragment field. The above analysis reveals that the force chain can provide essential information on the mechanical behavior of the sample. An advanced model is the basis for in-depth force chain network analysis.

The significance of the proposed model and force chain network analysis in relation to the mechanical properties and failure mechanisms of granite is as follows:

(1) Granites widely exist in various underground engineering projects and are a primary component of the surrounding rock to ensure the stability and safety of projects. Therefore, a suitable model that can reproduce the heterogeneous structure of granite on a 3D scale is necessary. In this modeling, the distinction of the mechanical behavior of different mineral structures is realized. Based on this model, all variables related to rock structure can be studied, not only the volume proportion of minerals studied in this paper but also the microscopic parameters, geometric size, and geometric shapes of minerals. The model proposed in this paper provides a simulation tool to determine the failure mechanism of rocks;

(2) A powerful tool reflecting the underlying mechanics driving the mechanical behavior of mineral structures is also necessary. To date, scholars have not found a suitable bridge for linking micromechanical information and macromechanical behavior. In this article, the strength of the force chain network in various structures of crystalline rocks is quantitatively analyzed. Based on the new analytical method, the influence of mineral structure on the load-bearing capacity of crystalline rocks is revealed. Compared with traditional force chain analysis, this approach realizes a leap from a qualitative description of phenomenology and experience to heterogeneous and refined quantitative research. This provides a foundation for related rock mechanics research in the future.

7. CONCLUSION

This study utilizes a three-dimensional grain-based model based on the discrete element method to replicate the heterogeneous structure of crystalline granite. In this model, not only is the mechanical behavior of different types of minerals distinguished, but the force chain network also realizes multilevel classification and quantitative analysis. Both the novel model and force chain analysis method are employed to quantitatively investigate the influence of mineral content on the mechanical behavior of granites. First, a set of granite specimens with varying biotite contents was constructed, and then, uniaxial compression tests were conducted. The effects of the mineral content on the mechanical behavior, force chain network characteristics, and fracture resistance of granite specimens were quantitatively analyzed. The main conclusions are summarized as follows:

(1) With increasing V_B, the quantity of basic elements representing biotite significantly increases, while the quantity of basic elements representing other types of minerals decreases. The contact number within the biotite structure significantly increases, while the contact numbers within the other intragranular structures decrease. When the contact number between two minerals increases, the contact number between the different minerals decreases.

(2) As V_B increases, the peak load of the specimens decreases, indicating an inverse relationship between the biotite content and the load-bearing capacity of the specimens under uniaxial compression conditions. The number of cracks

https://doi.org/10.1021/acsomega.3c09304
ACS Omega 2024, 9, 9603−9614

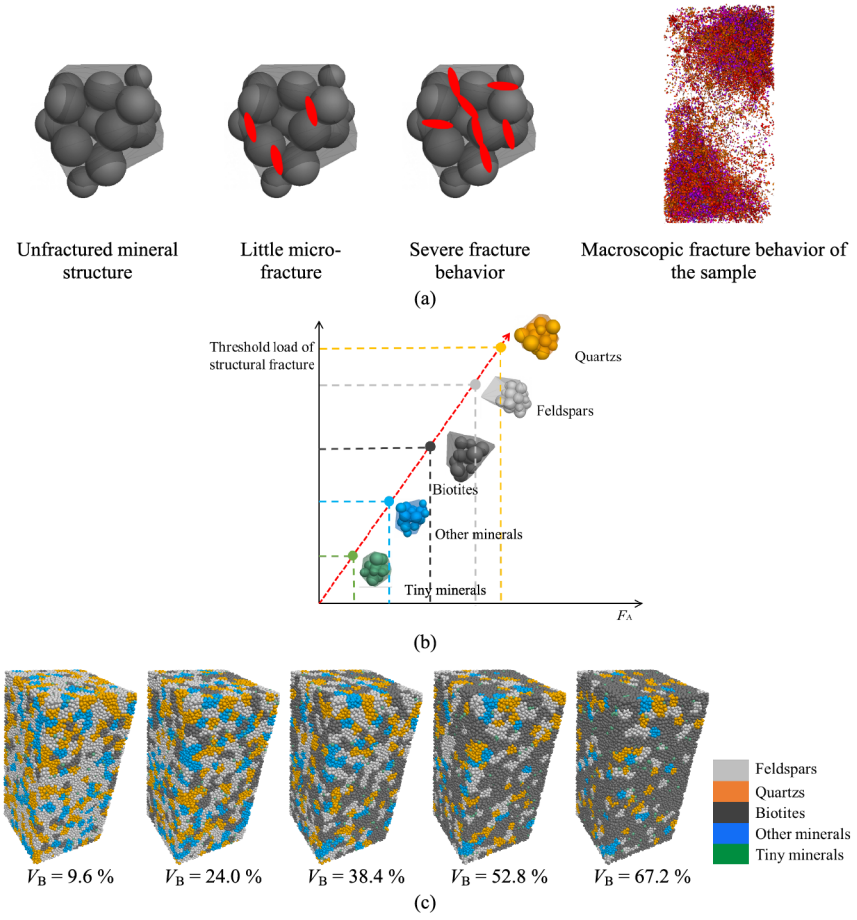

Figure 16. Relationship between fracture resistance of mineral structure and load-bearing capacity of granite: (a) fracture process of mineral grains and numerical samples; (b) fracture resistance and threshold load of structural fracture; (c) mineral distribution of samples with different biotite contents in this study.

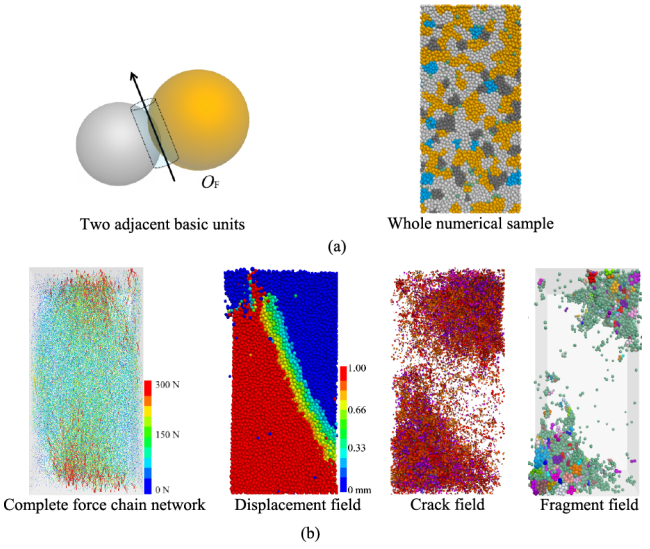

Figure 17. Description of the significance of force chain network: (a) basic elements and numerical sample; (b) influence of force chain network on deformation, microfracture, and macrofracture of sample.

within the biotite structure significantly increases, while the number of cracks of other types decreases. As V_B increases, the distribution density of force chains within the biotite structure increases, while the distribution density within other intragranular structures decreases. The average value and sum value of all of the force chains decrease with increasing V_B.

(3) Among the various structures considered, intragranular structures exhibit the highest fracture resistance, while intergranular structures exhibit a lower fracture resistance. The resistance to fracture of various mineral structures is ranked from largest to smallest according to the quartz, feldspar, biotite, other minerals, and fine minerals. When the proportion of biotite inside the sample increases, macrofracturing of the sample occurs under a lower load.

(4) Based on the novel force chain method, the influence of the mineral structure on the load-bearing capacity of crystalline rocks is revealed. Compared with traditional force chain analysis, this approach realizes a leap from a qualitative description of phenomenology and experience to heterogeneous and refined quantitative research. The micromechanical information and macromechanical behavior of rock materials can be linked. This might influence future research or practical applications in industries related to geotechnical engineering or construction.

AUTHOR INFORMATION

Corresponding Author

Wei Li − *Yunlong Lake Laboratory of Deep Underground Science and Engineering, Xuzhou, Jiangsu 221008, China; State Key Laboratory for Geomechanics and Deep Underground Engineering, China University of Mining and*

https://doi.org/10.1021/acsomega.3c09304
ACS Omega 2024, 9, 9603−9614

Technology, Xuzhou, Jiangsu 221116, China; orcid.org/0009-0001-1795-1596; Email: tbh259@cumt.edu.cn

Authors

Peigang Geng − *School of Transportation Engineering, Jiangsu Vocational Institute of Architectural Technology, Xuzhou, Jiangsu 221100, China*

Fangbin Zhao − *Xuzhou Metro Group Co., Ltd, Xuzhou, Jiangsu 221000, China*

Jie Zhang − *Yunlong Lake Laboratory of Deep Underground Science and Engineering, Xuzhou, Jiangsu 221008, China; State Key Laboratory for Geomechanics and Deep Underground Engineering, China University of Mining and Technology, Xuzhou, Jiangsu 221116, China*

Jingwei Liu − *Yunlong Lake Laboratory of Deep Underground Science and Engineering, Xuzhou, Jiangsu 221008, China; State Key Laboratory for Geomechanics and Deep Underground Engineering, China University of Mining and Technology, Xuzhou, Jiangsu 221116, China*

Complete contact information is available at: https://pubs.acs.org/10.1021/acsomega.3c09304

Notes

The authors declare no competing financial interest.

■ ACKNOWLEDGMENTS

The research presented in this paper was carried out under the financial support of the National Natural Science Foundation of China (Grant No. 52209151), Xuzhou City Science and Technology Innovation Special Basic Research Plan (KC23045), Yunlong Lake Laboratory of Deep Underground Science and Engineering Project (104023002). The authors would like to thank their colleagues of the Rock Mechanics research group at the China University of Mining and technology and Army Engineering University of PLA for technical discussion and comments.

■ REFERENCES

(1) Tian, W. L.; Yang, S. Q.; Wang, J. G.; Zeng, W. Numerical simulation of permeability evolution in granite after thermal treatment. *Comput. Geotech.* **2020a**, *126*, 103705.

(2) Tian, W. L.; Yang, S. Q.; Elsworth, D.; Wang, J. G.; Li, X. Z. Permeability evolution and crack characteristics in granite under treatment at high temperature. *Int. J. Rock Mech. Min. Sci.* **2020b**, *134* (76), 104461.

(3) Mahdi, S.; Taheri, A. A numerical approach to investigate the effects of rock texture on the damage and crack propagation of a pre-cracked granite. *Comput. Geotech.* **2019**, *111*, 89−111.

(4) Zhu, Z. N.; Tian, H.; Mei, G.; Jiang, G. S.; Bin, D. Experimental investigation on physical and mechanical properties of thermal cycling granite by water cooling. *Acta Geotechnica* **2019**, *15* (5), 1881−1893.

(5) Ju, M. H.; Li, X. F.; Li, X.; Zhang, G. L. A review of the effects of weak interfaces on crack propagation in rock: From phenomenon to mechanism. *Eng. Fract. Mech.* **2022b**, *263*, 108297.

(6) Yu, L. Y.; Zhang, T.; Wu, D. Y.; Wu, B. B.; Ma, L. J.; Wei, J. B. Numerical Investigation of the Effect of Grain Size-to-particle Size Ratio on the Dynamic Fracture Toughness of Granite by Using PFC3D-GBM. *Geomech. Geophys. Geo-Energy Geo-Resources* **2022**, *8*, 72.

(7) Zhang, T.; Yu, L. Y.; Peng, Y. X.; Jing, H. W.; Su, H.; Wei, J. Effect of the Mineral Spatial Distribution Heterogeneity on the Tensile Strength of Granite: Insights from PFC3D-GBM Numerical Analysis. *J. Rock Mech. Geotech. Eng.* **2023**, *15* (5), 1144−1160.

(8) Tandon, R. S.; Gupta, V. The control of mineral constituents and textural characteristics on the petrophysical & mechanical (PM) properties of different rocks of the Himalaya. *Eng. Geol.* **2013**, *153*, 125−143.

(9) Miskovsky, K.; Duarte, M. T.; Kou, S. Q.; Lindqvist, P.-A. Influence of the mineralogical composition and textural properties on the quality of coarse aggregates. *J. Mater. Eng. Perform.* **2004**, *13* (2), 144−150.

(10) Chen, L. X.; Guo, W. Y.; Jiang, Y. J.; Zhang, Y. Y.; Lu, D.; Han, F. Experimental study on influence of lithology on directional propagation law of type-I cracks. *J. Central South Univ.* **2023**, *30*, 3322−3334.

(11) Zhao, T. B.; Zhang, P. F.; Guo, W. Y.; Gong, X. F.; Wang, C.; Chen, Y. Controlling roof with potential rock burst risk through different pre-crack length: mechanism and effect research. *J. Central South Univ.* **2022**, *29* (11), 3706−3719.

(12) Zhang, W.; Guo, W. Y.; Wang, Z. Q. Influence of lateral pressure on the mechanical behavior of different rock types under biaxial compression. *J. Central South Univ.* **2022f**, *29* (11), 3695−3705.

(13) Ju, M. H.; Li, J. C.; Zhao, J. Transverse cracking of rock with a dissimilar inclusion under tension: effect of loading rate and inclusion diameter. *Rock Mech. Rock Eng.* **2022a**, *55* (9), 5513−5534.

(14) Si, X. F.; Luo, Y.; Luo, S. Influence of lithology and bedding orientation on failure behavior of "D" shaped tunnel. *Theor. Appl. Fract. Mech.* **2024**, *129*, 104219.

(15) Hu, L. H.; Su, G. S.; Liang, X.; Li, Y.; Yan, L. A distinct element based two-stage-structural model for investigation of the development process and failure mechanism of strainburst. *Comput. Geotech.* **2020**, *118*, 103333.

(16) Ju, M. H.; Wang, D. P.; Shi, J. C.; Li, J. C.; Yao, Q. L.; LI, X. Physical and numerical investigations of bedding adhesion strength on stratified rock roof fracture with longwall coal mining. *Geomech. Geophys. Geo-Energy Geo-Resources* **2021**, *7* (1), 24.

(17) Hu, L. H.; Yu, L. Y.; Ju, M. H.; Li, X. Z.; Tang, C. A. Effects of intermediate stress on deep rock strainbursts under true triaxial stresses. *J. Rock Mech. Geotech. Eng.* **2023**, *15* (3), 659−682.

(18) Zhao, J. S.; Duan, S. Q.; Chen, B. R.; Li, L.; He, B. G.; Li, P. X.; Liu, G. F. Failure mechanism of rock masses with complex geological conditions in a large underground cavern: A case study. *Soil Dyn. Earthquake Eng.* **2024**, *177*, 108439.

(19) Li, X. B.; Zou, Y.; Zhou, Z. L. Numerical simulation of the rock SHPB test with a special shape striker based on the discrete element method. *Rock Mech. Rock Eng.* **2014**, *47* (5), 1693−1709.

(20) Xu, Y.; Dai, F.; Xu, N. W.; Zhao, T. Numerical investigation of dynamic rock fracture toughness determination using a semi-circular bend specimen in split Hopkinson pressure bar testing. *Rock Mech. Rock Eng.* **2016**, *49* (3), 731−745.

(21) Huang, Y. H.; Yang, S. Q.; Ranjith, P. G.; Zhao, J. Strength failure behavior and crack evolution mechanism of granite containing pre-existing non-coplanar holes: Experimental study and particle flow modeling. *Comput. Geotech.* **2017**, *88*, 182−198.

(22) Du, H. B.; Dai, F.; Xu, Y.; Liu, H. N.; Xu, H.-N. Numerical investigation on the dynamic strength and failure behavior of rocks under hydrostatic confinement in SHPB testing. *Int. J. Rock Mech. Min. Sci.* **2018**, *108*, 43−57.

(23) Zhang, T.; Yu, L. Y.; Su, H. J.; Zhang, Q.; Chai, S. B. Experimental and numerical investigations on the tensile mechanical behavior of marbles containing dynamic damage. *Int. J. Min. Sci. Technol.* **2022b**, *32* (1), 89−102.

(24) Yang, S.; Tian, W.; Huang, Y.; Ranjith, P. G.; Ju, Y. An Experimental and Numerical Study on Cracking Behavior of Brittle Sandstone Containing Two Non-coplanar Fissures Under Uniaxial Compression. *Rock Mech. Rock Eng.* **2016**, *49* (4), 1497−1515.

(25) Potyondy, D. O.; Cundall, P. A. A bonded-particle model for rock. *Int. J. Rock Mech. Min. Sci.* **2004**, *41* (8), 1329−1364.

(26) Peng, J.; Wong, L. N. Y.; Cee, I. T. Influence of grain size heterogeneity on strength and microcracking behavior of crystalline rocks. *J. Geophy. Res.: Solid Earth* **2016**, *122* (2), 1054−1073.

(27) Peng, J.; Wong, L. N. Y.; Teh, C. I. CEE IT. A re-examination of slenderness ratio effect on rock strength: Insights from DEM grain-based modelling. *Eng. Geol.* **2018**, *246*, 245−254.
(28) Li, X. F.; Li, H. B.; Zhao, J. Transgranular fracturing of crystalline rocks and its influence on rock strengths: Insights from a grain-scale continuum−discontinuum approach. *Comput. Methods Appl. Mech. Eng.* **2021**, *373*, 113462.
(29) Li, X. F.; Zhang, Q. B.; Li, H. B.; Zhao, J. Grain-Based Discrete Element Method (GB-DEM) Modelling of Multi-scale Fracturing in Rocks Under Dynamic Loading. *Rock Mech. Rock Eng.* **2018**, *51* (12), 3785−3817.
(30) Saadat, M.; Taheri, A. Modelling Micro-cracking Behaviour of Pre-cracked Granite Using Grain-Based Distinct Element Model. *Rock Mech. Rock Eng.* **2019**, *52* (11), 4669−4692.
(31) Zhang, T.; Yu, L. Y.; Li, J.; Ma, L. J.; Su, H. J.; Zhang, M. W.; Xu, X. L.; Peng, Y. X. Numerical Investigation of the Effects of the micro-parameters of the transgranular contact on the mechanical response of granite. *Theor. Appl. Fract. Mech.* **2022c**, *118*, 103259.
(32) Zhang, T.; Yu, L. Y.; Peng, Y. X.; Ju, M. H.; Yin, Q.; Wei, J. B.; Jia, S. P. Influence of Grain Size and Basic Element Size on Rock Mechanical Characteristics: Insights from Grain-based Numerical Analysis. *Bull. Eng. Geol. Environ.* **2022d**, *81* (9), 347.
(33) Zhang, T.; Yu, L. Y.; Ju, M. H.; Jing, H. W.; Su, H. J.; Wei, J. B.; Peng, Y. X.Effect of Grain Size on the Dynamic Flexural Tensile Strength of Granite: Insight from GBM3D-PFC Simulations*Int. J. Geomech.***2023***235*
(34) Dantu, P.Contribution a l'etude mecanique et geometrique des milieux pulverulents*Proceedings of the 4th International Conference on Soil Mechanics and Foundation Engineering***1957***1*144148
(35) Edwards, S. F.; Oakeshott, R. B. S. Theory of powders. *Phys. A Stat. Mech. Appl.* **1989**, *157* (3), 1080−1090.
(36) Bouchaud, J. P.; Cates, M. E.; Claudin, P. Stress distribution in granular media and nonlinear wave equation. *J. Phys. I* **1995**, *5* (6), 639−656.
(37) Zhao, K.; Wu, W. K.; Zeng, P.; Yang, D. X.; Liu, Y. G.; Wang, L.; Ran, S. H. Numerical and experimental assessment of the sandstone fracture mechanism by non-uniform bonded particle modeling. *Rock Mech. Rock Eng.* **2021**, *54* (12), 6023−6037.
(38) Poulsen, B. A.; Adhikary, D. P. A numerical study of the scale effect in coal strength. *Int. J. Rock Mech. Min. Sci.* **2013**, *63*, 62−71.
(39) Chen, B.; Xiang, J. S.; Latham, J.-P.; Bakker, R. R. Grain-scale failure mechanism of porous sandstone: An experimental and numerical FDEM study of the brazilian tensile strength test using CT-Scan microstructure. *Int. J. Rock Mech. Min. Sci.* **2020**, *132*, 104348.
(40) Nitka, M.; Tejchman, J. Comparative DEM calculations of fracture process in concrete considering real angular and artificial spherical aggregates. *Eng. Fract. Mech.* **2020**, *239* (147), 107309.
(41) Ding, X. B.; Zhang, L. Y.; Zhu, H. H.; Zhang, Q. Effect of model scale and particle size distribution on PFC3D simulation results. *Rock Mech. Rock Eng.* **2014**, *47*, 2139−2156.
(42) Yang, S. Q.; Yin, P. F.; Huang, Y. H. Experiment and Discrete Element Modelling on Strength, Deformation and Failure Behaviour of Shale Under Brazilian Compression. *Rock Mech. Rock Eng.* **2019**, *52* (11), 4339−4359.
(43) Yu, J.; Yao, W.; Duan, K.; Liu, X. Y.; Zhu, Y. L. Experimental study and discrete element method modeling of compression and permeability behaviors of weakly anisotropic sandstones. *Int. J. Rock Mech. Min. Sci.* **2020**, *134* (1), 104437.
(44) Wang, Q.; Hu, X. L.; Zheng, W. B.; Li, L. X.; Zhou, C.; Ying, C. Y.; Xu, C. Mechanical properties and permeability evolution of red sandstone subjected to hydro-mechanical coupling: experiment and discrete element modelling. *Rock Mech. Rock Eng.* **2021**, *54* (5), 2405−2423.
(45) Zhang, T.; Yu, L. Y.; Wu, B. B.; Tan, Y. Z.; Su, H. J.; Zhou, L. J. Influence of grain-to-particle size ratio on the tensile mechanical response of granite based on a novel three-dimensional grain-based model. *Eng. Fract. Mech.* **2022e**, *259*, 108161.
(46) Wei, J. B.; Wang, S. M.; Song, S. J.; Sun, Q.; Yang, T. Experiment and numerical simulation of overburden and surface damage law in shallow coal seam mining under the gully. *Bull. Eng. Geol. Environ.* **2022**, *81* (5), 1−17.
(47) Peng, Y. X.; Zhang, T.; Yu, L. Y.; Li, J.; Gao, Y. N.; Tian, W. L. Numerical Investigation on the Effect of Intergranular Contact Bonding Strength on the Mechanical Properties of Granite Using PFC3D-GBM. *Int. J. Numer. Anal. Methods Geomech.* **2023**, *47* (5), 694−716.

https://doi.org/10.1021/acsomega.3c09304
ACS Omega 2024, 9, 9603−9614